First-principles based analysis of thermal transport in metallic nanostructures: Size effect and Wiedemann-Franz law

Yue Hu, Shouhang Li, and Hua Bao ®*
*University of Michigan–Shanghai Jiao Tong University Joint Institute, Shanghai Jiao Tong University,
Shanghai 200240, People's Republic of China*

Metallic nanostructures (nanofilms and nanowires) are widely used in electronic devices, and their thermal transport properties are crucial for heat dissipation. However, there are still gaps in understanding thermal transport in metallic nanostructures, especially regarding the size effect and validity of the Wiedemann-Franz law. In this work, we perform mode-by-mode first-principles calculations combining the Boltzmann transport equation to understand the thermal transport in metallic nanostructures. We take gold (Au) and tungsten (W) nanostructures as prototypes. It is found that when the size of nanostructures is on the order of several tens of nanometers, the electronic/phonon thermal conductivity is smaller than the bulk value and decreases with size. The phonon contribution to the total thermal conductivity increases in nanostructures for those metals with small bulk phonon thermal conductivity (like Au), while it may increase or be suppressed in nanostructures for those metals with large bulk phonon thermal conductivity (like W). By assuming that the grain boundary does not induce inelastic electron-phonon scattering, the Wiedemann-Franz law works well in both Au and W nanostructures if the Lorentz ratio is estimated using electronic thermal conductivity. The Wiedemann-Franz law also works well in Au nanostructures when the Lorentz ratio is estimated by total thermal conductivity.

I. INTRODUCTION

Due to the miniaturization of electronic devices, metallic nanostructures (nanofilms and nanowires) play an imperative role in electronic applications ranging from interconnects to sensors [1–3]. Since effective heat dissipation is crucial to ensure the reliability of electronic devices [4], the thermal conductivity of metallic nanostructures is crucial [5–11]. Over the past two decades, there have been many discussions on thermal transport in metallic nanostructures [9,10,12–18]. Among these discussions, there are two key issues: the size effect and the validity of the Wiedemann-Franz law.

Both experimental and theoretical evidence shows a size effect [19,20]: the thermal conductivities in the metallic nanostructures are smaller than their bulk counterparts and depend on the size of the nanostructures. This size effect is attributed to the surface scattering and grain boundary scattering of the electron/phonon [21–23]. The size effect of the electronic component has been described by Fuchs-Sondheimer theory and Mayadas-Shatzkes theory [24,25]. However, the success of these theories relies on the validity of the free electron model [7]. For the phonon component, the main strategy used in previous works is roughly estimating the phonon thermal conductivity using the molecular dynamics method or the Debye model [26–29]. However, the magnitude of phonon thermal conductivity is still under debate. For example, in gold nanostructures, some studies believe that the phonon component can be ignored [5,9,27], while other studies estimate a large phonon component, which is even larger than the electronic component [7,15]. An established understanding of the size effect on phonon thermal conductivity is still lacking.

The Wiedemann-Franz law states that the ratio of the electronic thermal conductivity to the electrical conductivity in a metal is proportional to the temperature. The proportionality constant, known as the Lorentz ratio, is assumed to be the Sommerfeld value, $L_0 = 2.44 \times 10^{-8}$ W $\Omega/$K^2 [30]. When the phonon contribution is negligible, the Wiedemann-Franz law provides an estimation of thermal conductivity according to the measured electrical conductivity, which is easier to be measured [30]. Meanwhile, the Wiedemann-Franz law can be used to separate the electron and phonon contributions when the total thermal conductivity is known [8]. However, the validity of the Wiedemann-Franz law in metallic nanostructures is still controversial. Several researchers reported that the Lorentz ratio is several times larger than the Sommerfeld value [7,8,15,16,26], while other researchers reported the Lorentz ratio is around or smaller than the Sommerfeld value [9–11,18,31–33]. Moreover, it is still under debate whether or not the Lorentz ratio is size and temperature dependent [5,9,31]. Stojanovic *et al.* proposed that the deviation of the Lorentz ratio from the Sommerfeld value is related to the neglect of phonon contribution and the inelastic electron-phonon scattering [28]. A quantitative understanding of phonon contribution and inelastic electron-phonon scattering is desired to understand the Wiedemann-Franz law in metallic nanostructures.

*Author to whom correspondence should be addressed: hua.bao@sjtu.edu.cn

In this work, we tackle these two issues using a theoretical calculation combining first-principles calculations and Boltzmann transport equations. We take gold (Au) and tungsten (W) as testing materials, as their transport properties are widely studied in experiments [9,15,34,35]. Furthermore, the two metals have typical characteristics from a theoretical perspective (Au has a near spherical Fermi surface and W has a complicated Fermi surface [36,37]). Different from previous theoretical calculations [24,25,28], we consider the intrinsic electron and phonon properties using rigorous mode-by-mode first-principles calculations [37–39], instead of applying assumptions such as the free electron assumption and Debye model for the phonon [28]. Combining the Boltzmann transport equation with the intrinsic electron and phonon properties, the thermal transport properties (thermal conductivity and Lorentz ratio) of metallic nanostructures can be predicted.

II. METHOD AND SIMULATION DETAILS

In this section, we provide our calculation framework: first-principles calculations combining the Boltzmann transport equation for predicting the thermal conductivity of metallic nanostructures. Since our framework is based on the Boltzmann transport equation, we restricted our focus to length scales beyond ten nanometers, for which the quantum confinement effects of the electron or phonon can be ignored [40,41]. Both the electron and phonon are involved in the thermal transport of metallic nanostructures. The electron and phonon in nanostructures not only encounter intrinsic scattering processes in ideal bulk [36,38], but also encounter external scattering processes including surface scattering and grain boundary scattering [24,25].

A. Surface scattering and grain boundary scattering

Both surface scattering and grain boundary scattering are important in the phonon and electron transport in metallic nanostructures [24,25]. Schematics of these scattering processes as well as the typical structure of a nanofilm/nanowire with thickness/diameter H and average grain size D are shown in Fig. 1. The grain boundary is assumed to be perpendicular to the surface, as observed in the experimental samples [22,25]. The proportionality between the average grain size D and the thickness H is usually adopted in experiments, and the proportionality constant is usually in the range of 2–0.5 [22,25,42].

To describe the surface scattering, we adopt the idea of Fuchs' model: some of the carriers are specularly reflected by the surface, while others are diffusely reflected by the surface (Fig. 1). The percentage of specularly reflected carriers is specularity p. This model is also known as the partial diffuse-partial specular boundary condition, which is widely used in surface scattering modeling [43–45]. The specularity p for each electron or phonon λ can be obtained by Soffer's model [46,47],

$$p_\lambda = \exp\left(-16\pi^2\eta^2 / \Lambda_\lambda^2 \cos^2\theta\right),$$

where η is the roughness of the surface, and Λ_λ is the wavelength of the electron or phonon. θ is the incident angle.
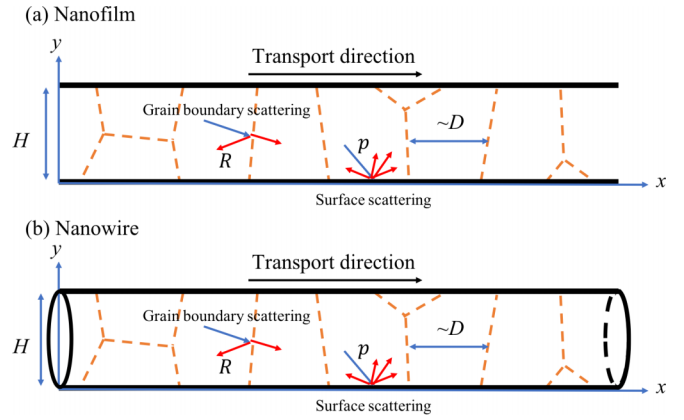

FIG. 1. Surface scattering and grain boundary scattering in a typical (a) nanofilm and (b) nanowire. The thickness of the nanofilm is H and the average grain size is D. The diameter of the nanowire is H and the average grain size is D. The specularity of carriers at the surface is p. The reflection coefficient of carriers at the grain boundary is R.

The roughness η of the surface can be measured, and the reported values are around 1 nm [22,48,49]. For Au and W, the wavelengths of electrons and phonons contributing 80% of thermal conductivity are smaller than 1 nm. According to Soffer's model, when the roughness is around 1 nm, the specularity is nearly zero (pure diffuse surface scattering) for all electrons and phonons in both Au and W. Thus, we assume a diffuse surface scattering for all carriers in subsequent sections.

The scattering around the grain boundary is complex and similar to the scattering at the interface [50,51]. To simplify the complex grain boundary scattering, we adopt the idea of Mayadas' model: some of the carriers transmit across the grain boundary, while others are reflected at the grain boundary. The percentage of reflected carriers is the reflection coefficient R [25]. The accuracy of this model depends on the reflection coefficient. As far as we know, it is difficult to theoretically obtain the reflection coefficient R, which is usually obtained by fitting the experimental results [27,42,52]. The range of reported R for electrons is 0.2–0.8 for polycrystalline nanostructures [8,27,28,53]. The large range may be due to the fact that R is related to the configuration of the grains, which varies for different samples. Previous studies demonstrated that the grain boundary resistance for phonon transport is low (much lower than that for electronic transport) [54,55], thus we assume that all phonons can transmit across the grain boundaries, i.e., the reflection coefficients of phonon modes are zero [28].

Since the structural scatterings are usually treated as elastic scattering [56–58], we assume the charge and thermal transport of the electron have the same specularity and reflection coefficient.

B. Thermal conductivity: Boltzmann transport equation model

By solving the Boltzmann transport equation with the relaxation time approximation [19], the phonon and electronic

thermal conductivity in the transport direction of a metallic nanostructure (nanofilm or nanowire) can be calculated as

$$\kappa = \sum_\lambda c_\lambda \|v_{x,\lambda}\|^2 \tau_\lambda S_\lambda, \tag{1}$$

where κ is the phonon thermal conductivity $\kappa_{\rm ph}$ or the electronic thermal conductivity κ_e. For the phonon thermal conductivity, $\lambda \equiv (\mathbf{q}, \upsilon)$ denotes the phonon mode with polarization υ and wave vector $\mathbf{q}$. For the electronic thermal conductivity, the $\lambda \equiv (\mathbf{k}, n)$ denotes the electron with wave vector $\mathbf{k}$ and band index n. c_λ is the volumetric specific heat

of the phonon or the electron. $v_{x,\lambda}$ denotes the component of the phonon group velocity or the electron velocity in the transport direction. τ_λ denotes the intrinsic phonon relaxation time or the intrinsic electronic thermal transport relaxation time. S_λ denotes the "suppression function" for phonons and electrons, which captures the size dependence of the thermal conductivity. For bulk materials, S_λ is equal to 1, and Eq. (1) is reduced to the expression for bulk materials [59]. Thus, Eq. (1) can be simplified as $\kappa = \sum_\lambda \kappa_{{\rm bulk},\lambda} S_\lambda$. S_λ for nanofilms and nanowires are related to surface scattering and grain boundary scattering. For the nanofilm, S_λ is expressed as

$$S_\lambda(H, D, \tau_\lambda, v_\lambda, p_\lambda, R) = \frac{\tau'_\lambda}{\tau_\lambda} \frac{1}{H} \int_0^H \left[1 - \frac{1 - p_\lambda}{1 - p_\lambda \exp(-H/\tau'_\lambda|v_{y,\lambda}|)} \exp\left(-\frac{y}{\tau'_\lambda|v_{y,\lambda}|}\right) \right] dy, \tag{2}$$

where τ'_λ is the relaxation time considering the intrinsic scattering processes (electron-phonon, phonon-phonon, and phonon-electron scattering) and grain boundary scattering process, and is expressed as

$$\frac{1}{\tau'_\lambda} = \frac{1}{\tau_\lambda} + \frac{\alpha}{2\tau_\lambda} \frac{v_\lambda}{|v_{\lambda,x}|}, \quad \alpha = \frac{v_\lambda \tau_\lambda}{D} \frac{R}{1-R}. \tag{3}$$

According to the expression, when the reflection coefficient is nearly 0 (all carriers can transmit the grain boundary) or the mean free path is much smaller than the grain size, the grain boundary scattering can be ignored and τ'_λ is equal to the intrinsic relaxation time τ_λ. Since we have assumed the reflection coefficients of phonon modes to be zero, the grain boundary scattering of phonons is ignored. The electron/phonon properties including velocity, heat capacity, and intrinsic relaxation time are obtained by first-principles calculations. The detailed derivation of Eq. (2) as well as the equation for nanowires are presented in the Supplemental Material [60].

The formula above can also be used in electrical conductivity calculation, i.e., $\sigma = \sum_\lambda \sigma_{{\rm bulk},\lambda} S_\lambda$, which will not be discussed here.

C. Intrinsic phonon and electron properties: First-principles calculations

For phonons, the volumetric specific heat can be obtained by $c_{{\rm v},\lambda} = \frac{\hbar\omega_\lambda}{V} \frac{\partial n_\lambda^0}{\partial T}$, with n_λ^0 the Bose-Einstein distribution function, V the volume of the primitive cell, ω_λ the phonon frequency, and T the temperature. The phonon group velocity can be obtained by $\mathbf{v}_\lambda = \frac{\partial \omega_\lambda}{\partial \mathbf{q}}$. The phonon relaxation time can be obtained using the Matthiessen's rule [61] considering both phonon-phonon and phonon-electron scattering [62], namely $1/\tau_\lambda = 1/\tau_{pp} + 1/\tau_{pe}$, where $1/\tau_{pp}$ is the scattering rate with respect to three-phonon interactions [61], and $1/\tau_{pe}$ is the scattering rate with respect to phonon-electron interactions [63]. For electrons, the volumetric specific heat can be obtained by $c_{{\rm v},n\mathbf{k}} = -\frac{n_s}{VT}(\varepsilon_{n\mathbf{k}} - \mu)\frac{\partial f_{n\mathbf{k}}^0}{\partial \varepsilon_{n\mathbf{k}}}$, with $f_{n\mathbf{k}}^0$ the Fermi-Dirac distribution function, V is the volume of the primitive cell, n_s denotes spin degeneracy, $\varepsilon_{n\mathbf{k}}$ is the electron energy, and μ is the Fermi energy. It should be noted that we

only consider the zero-electric-field condition for electronic thermal conductivity and heat capacity and ignore the effects of electrochemical potential gradient. This is reasonable for metals since the reduction of electronic thermal conductivity caused by the thermoelectric effects is usually smaller than 1%. However, the thermoelectric effects cannot be ignored in semiconductors and the zero-current formula should be used. The electron group velocity can be obtained by $\mathbf{v}_{n\mathbf{k}} = \frac{1}{\hbar}\frac{\partial\varepsilon_{n\mathbf{k}}}{\partial\mathbf{k}}$. For pure metals at intermediate and high temperatures, the electron relaxation time is limited by electron-phonon scattering and can be obtained using Fermi's "golden rule" [64]. In particular, we rigorously consider the elastic/inelastic electron-phonon scatterings and their effects on transport coefficients by distinguishing the electron relaxation time for heat and charge transport. More computational details of the intrinsic phonon and electron properties (for both heat and charge transport) from first-principles methods have been described previously [38]. The electron relaxation time approximation is employed to obtain the electrical transport properties of metals in this work. The electron relaxation times are well defined and the results calculated by this method are close to experimental data [38]. Similar numerical results can also be obtained using the iterative calculation scheme [36,65,66].

We carried out the first-principles calculations using the QUANTUM ESPRESSO [67] package to predict electron transport. The types of local density approximation (LDA) [68] and generalized gradient approximation (GGA) [69] exchange-correlation functional are used for Au and W, respectively. The phonon-phonon scattering rate is evaluated by the SHENG-BTE package [70]. The harmonic force constants are extracted using density functional perturbation theory (DFPT) with a $6 \times 6 \times 6$ $\mathbf{q}$-point mesh. A supercell of $4 \times 4 \times 4$ and the third nearest atom neighbor is considered to obtain the cubic force constants [70]. The $\mathbf{q}$-point mesh is set as $60 \times 60 \times 60$ and $40 \times 40 \times 40$ in the BTE solver, respectively for Au and W to ensure the convergence of lattice thermal conductivity. The phonon-electron scattering rate and electron-phonon scattering rate are evaluated using the EPW package [71]. The cutoff energy of plane wave is set as 180 Ry for Au and 120 Ry for W. A threshold of energy of 10^{-10} Ry is employed in the self-consistent field calculation and non-self-
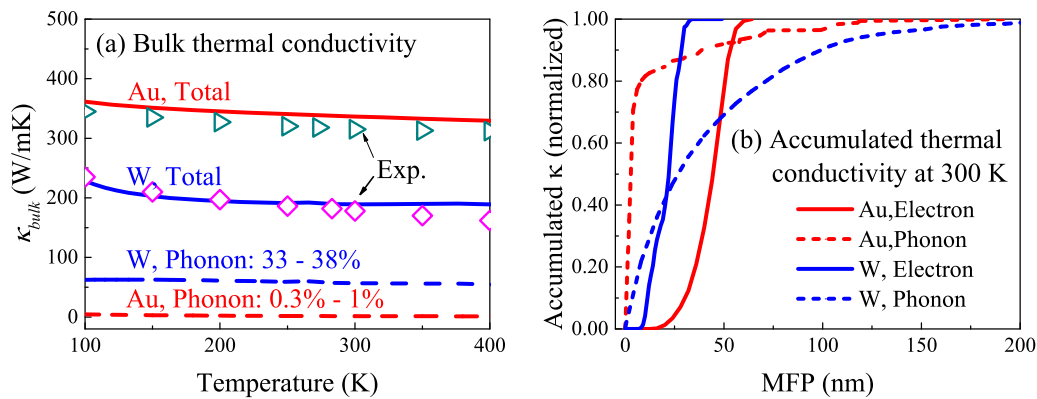
FIG. 2. (a) Bulk thermal conductivity of Au and W. The experimental data are taken from Ref. [72]. (b) The normalized thermal conductivity accumulation with respect to carrier mean free path (MFP) in Au and W at 300 K.

consistent field calculation. The initial coarse **k**-point and **q**-point meshes are set as $12 \times 12 \times 12$ and $6 \times 6 \times 6$, respectively, for both Au and W. The **k**-point and **q**-point meshes are set to be $80 \times 80 \times 80$ and $60 \times 60 \times 60$ for Au, while $100 \times 100 \times 100$ and $40 \times 40 \times 40$ for W to sample the Brillouin zone.

D. Bulk thermal conductivity and mean free path

We present the bulk thermal conductivity for Au and W in Fig. 2(a), calculated by Eq. (1) (the suppression function S_λ is equal to 1). The calculated bulk thermal conductivity agrees well with the experimental results [72] (the error is less than 10%). In bulk Au, the phonon contribution is negligible (less than 1% of the total thermal conductivity). In contrast, in bulk W, the phonon contribution is more than 30% of the total thermal conductivity.

The thermal conductivity accumulation [73] with respect to the carrier mean free path at 300 K is shown in Fig. 2(b). This property is crucial for our mode-by-mode calculation. This also shows that our model is more accurate than previous studies, which usually adopt the averaged electron MFP from the free electron model and phonon thermal conductivity from molecular dynamics or the Debye model [15,28]. In general, the range of electron mean free path is much narrower than that of the phonon mean free path for both Au and W. In Au, 80% of the phonon thermal conductivity is contributed by phonons with mean free path less than 10 nm, which is smaller than the mean free path of the electron. In W, above 50% of the phonon thermal conductivity is contributed by the phonon with mean free path larger than 25 nm, which is larger than the mean free path of the electron. At lower temperatures, the mean free path of carriers becomes larger [36,39], which is not shown here for simplicity.

III. SIZE EFFECT

In this section, we study the size effect of the total thermal conductivity, electronic thermal conductivity, phonon thermal conductivity, and the phonon contribution. We only present the results for nanofilms in the main text and the results for nanowires are presented in the Supplemental Material [60].

All the conclusions about nanofilms can also be applied to nanowires.

A. Total thermal conductivity

In this subsection, we study the size effect of total thermal conductivity in Au and W nanofilms (including single-crystalline and polycrystalline nanofilms) at 300 and 100 K. Previous studies demonstrated that the electrical conductivity in W single-crystalline nanofilms is related to the transport orientation [59,60]. Thus, we study the single crystalline for [100] and [110] transport orientations. Polycrystalline nanostructures always relate to multiple orientations and thus we assume a random distribution of orientations in calculating grain boundary scattering (in polycrystalline nanofilms). As described in Sec. II A, we assume the pure diffuse surface scattering. For polycrystalline nanofilms, we present the data for grain size D equal to the thickness H and electron reflection coefficient R equal to 0.5. Other D/H values and electronic R values will be discussed later.

The normalized total thermal conductivity (over the bulk total thermal conductivity) values are shown in Fig. 3. For all nanofilms, the thermal conductivity is smaller than 90% of the bulk value for sizes ranging from 400 to 20 nm. Since the mean free path of the carriers contributing 80% thermal conductivity is on the order of magnitude 10 nm, the size effect is obvious when the size is less than ten times the mean free path [24,25,74]. When the size decreases, the thermal conductivity of the nanofilm decreases. At 300 K, the thermal conductivity reduces to 20% of the bulk value for the 20-nm Au polycrystalline nanofilm and 35% of the bulk value for the 20-nm W polycrystalline nanofilm [Figs. 3(a) and 3(c)]. Since the mean free path of carriers increases with temperature decreasing, the reduction of thermal conductivity is larger at 100 K and reaches 90% for the 20-nm Au polycrystalline nanofilm and 80% for the 20-nm W polycrystalline nanofilm. Compared with polycrystalline nanofilms, the reduction is smaller in the single-crystalline nanofilm (50% reduction for the 20-nm Au nanofilm and 40% reduction for the 20-nm W nanofilm at 300 K) due to the absence of electron grain boundary scattering [Figs. 3(b) and 3(d)]. In single-crystalline nanofilms, the thermal conductivity is transport orientation dependent. The
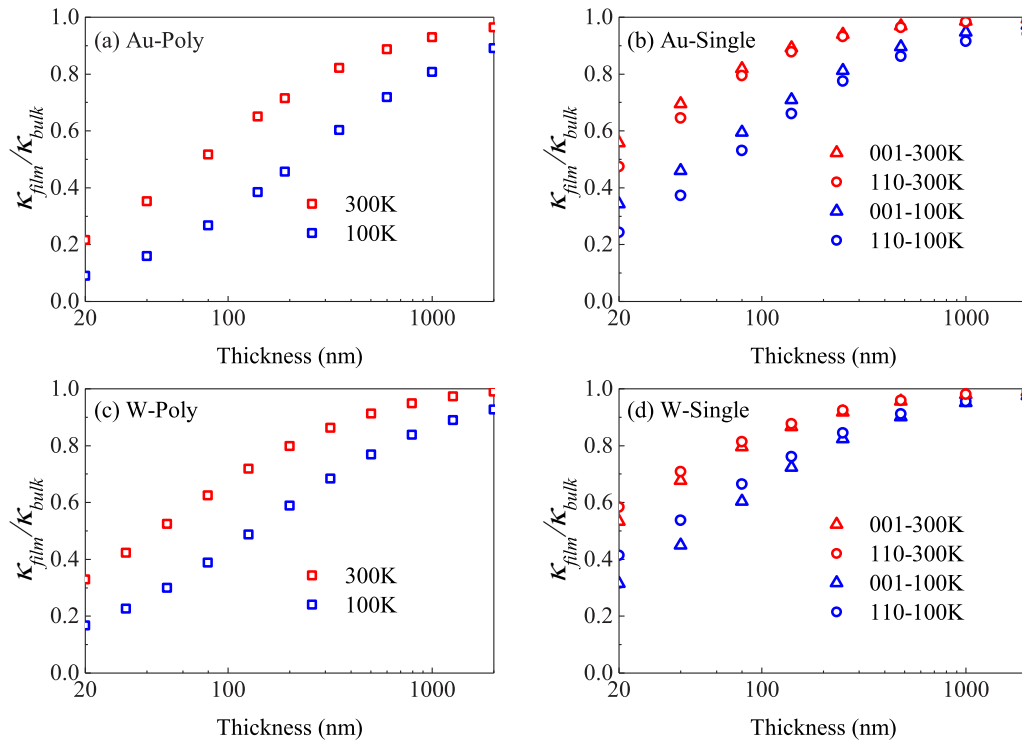
FIG. 3. Thickness H dependence of normalized thermal conductivity over bulk thermal conductivity for the (a) polycrystalline Au nanofilm, (b) single-crystalline Au nanofilm, (c) polycrystalline W nanofilm, and (d) single-crystalline W nanofilm.

difference between the two orientations increases when the size decreases. However, compared with the large reduction of thermal conductivity from bulk values (around 50% at 20 nm), the difference between these two orientations is not large (less than 10% of the bulk thermal conductivity at 20 nm). This anisotropy of thermal conductivity is similar to the anisotropy of electrical conductivity observed in previous work, which is due to the anisotropy of the Fermi surface [75].

In the following subsections, we analyze the size effect of the electron component and the phonon component separately. Since the polycrystalline nanofilms are usually fabricated in experiments and contain both surface and grain boundary scattering [8], we will only present the data for polycrystalline nanofilms in the remaining parts.

B. Electronic thermal conductivity

As described in Sec. II A, we assume pure diffuse surface scattering. The ratio of the grain size to the thickness D/H ranges from 0.5 to 2. The electron reflection coefficient R ranges from 0.2 to 0.8. The range of corresponding thermal conductivity at 300 K is shown by the shadow region in Fig. 4. We also present the typical values corresponding to $D/H = 1$ and $R = 0.5$ in Fig. 4 as dots. At 300 K, the electronic thermal conductivity is reduced to 90% of the bulk value when the size is smaller than 400 nm for Au and 200 nm for W. This can happen as the electron mean free path is around 40 nm for Au and 20 nm for W. When the thickness decreases, the electronic thermal conductivity decreases. At 300 K, the thermal conductivity reduces to 20% for the 20-nm Au nanofilm and 40% for the 20-nm W nanofilm. Because the mean free path of electrons increases with temperature decreases, this reduction is larger at 100 K and around 90% for both Au and W at 20 nm. When D/H decreases or R increases, the electronic thermal conductivity decreases due to the larger grain boundary scattering. At 300 K, for D/H ranging from 0.5 to 2 and R ranging from 0.2 to 0.8, the reduction of electronic thermal conductivity goes from 55% to 98% for Au nanofilm and from 40% to 90% for W nanofilm with a thickness of 20 nm.

The free electron model has been widely used in previous theoretical works [24,25]. However, whether or not it is good at metallic nanostructure properties prediction remains unknown. In this model, one assumes that the velocities of all electrons are the Fermi velocity (1.39×10^6 m/s for Au and 6.1×10^5 m/s for W [76,77]); the Fermi surface is spherical, and the mean free path of all electrons is the same, which is the averaged mean free path calculated by $l_F = \kappa_{e,\mathrm{bulk}}/(\frac{1}{3}c_e v_F))$. It should be noted that this free electron model uses the electronic thermal conductivity calculated from real electron and phonon modes. The average mean free path of electrons is 45 nm for Au and 22 nm for W at 300 K (the average mean free paths from 100 to 400 K are presented in the Supplemental Material [60]). We also calculate the electronic thermal conductivity using the free electron model. The results from the free electron model match the mode-by-mode results well (the error is smaller than 10% for both Au and W, Fig. 4). This observation is also valid for other D/H values, R values, and other temperatures between 100 and 400 K, which are not shown here for simplicity. This phenomenon is due to the fact that the range of electron mean free paths is not large for both W and Au (Fig. 2).
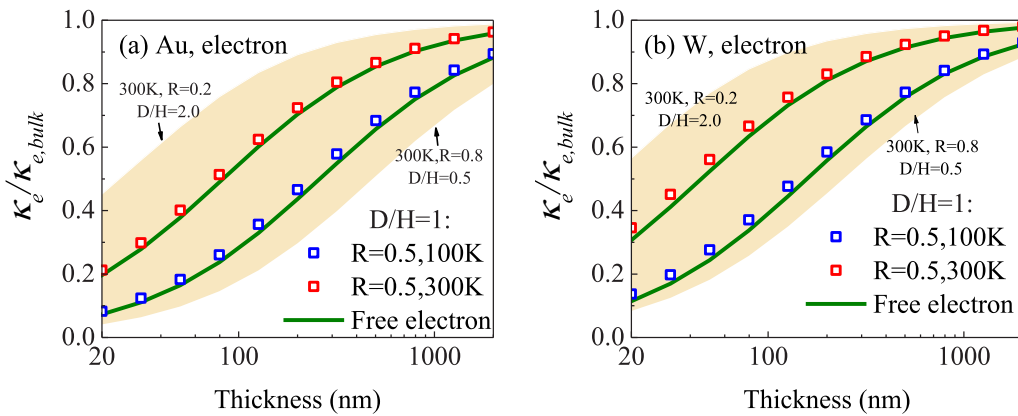
FIG. 4. Thickness H dependent electronic thermal conductivity over bulk electronic thermal conductivity for the (a) Au nanofilm and (b) W nanofilm.

C. Phonon thermal conductivity

In this subsection, we discuss the size effect on phonon thermal conductivity. As described in Sec. II A, we assume pure diffuse surface scattering and ignore the grain boundary scattering of phonons. The reduction of the phonon thermal conductivity for the 20-nm Au nanofilm is only 17% at 300 K [Fig. 5(a)], since the mean free path of the phonon is only around 2 nm [Fig. 2(b)]. The reduction reaches 30% at 100 K due to the increase in the mean free path. In contrast, the reduction in phonon thermal conductivity for W is much larger [Fig. 5(b)]. The thermal conductivity is reduced to 90% of the bulk value when the size is smaller than 700 nm at 300 K. This phenomenon is related to the large mean free path of phonon in W, which spans from several nanometers to 200 nm. The reduction reaches 70% for the 20-nm W nanofilm. The reduction increases further at lower temperatures.

Apart from the value of phonon thermal conductivity, the percentage of phonon thermal conductivity contributing to the total thermal conductivity (phonon contribution) also receives attention [36,37]. Thus, we present the percentage of phonon thermal conductivity in Fig. 6. We also present the range of the phonon contribution as the shadow region and the typical values corresponding to $D/H = 1$ and electron $R = 0.5$ as dots. In general, the $\kappa_{ph}/\kappa_{total}$ in nanofilms can be much different from that in bulk. For Au, the phonon contribution

is larger in nanofilms than in bulk and increases with the size decreases [Fig. 6(a)]. For $D/H = 1$ and electron $R = 0.5$, the $\kappa_{ph}/\kappa_{total}$ increases to 1% for the 20-nm Au nanofilm at 300 K. This percentage further increases with temperature decreases, the grain size decreases and the reflection coefficient of electrons increases. At 100 K, the $\kappa_{ph}/\kappa_{total}$ can reach up to 12%, which is much larger than 1% in bulk. The increment of the phonon contribution in Au nanofilms is due to the smaller size effect of the phonon part than that of the electron part, which is caused by two facts: (1) the phonon mean free path is smaller than the electron mean free path in Au [Fig. 2(b)]; (2) the phonon reflection coefficient is smaller than the electron reflection coefficient (0 versus 0.2–0.8). At lower temperatures, the larger size effect further increases the phonon contribution. In contrast, for W, the $\kappa_{ph}/\kappa_{total}$ is larger in some nanofilms and smaller in other nanofilms compared with in bulk W [Fig. 6(b)]. For $D/H = 1$ and electron $R = 0.5$, the percentage is smaller in the 20-nm W nanofilm (30%) than in the bulk value (35%) at 300 K. However, at 100 K, the percentage is larger in 20-nm W nanofilm (45%) than in the bulk value (33%). The reason for this is the trade-off between the larger phonon mean free path versus the electron mean free path [Fig. 2(b)] and the smaller phonon reflection coefficient versus the electron reflection coefficient. The former causes a larger size effect in phonons than in
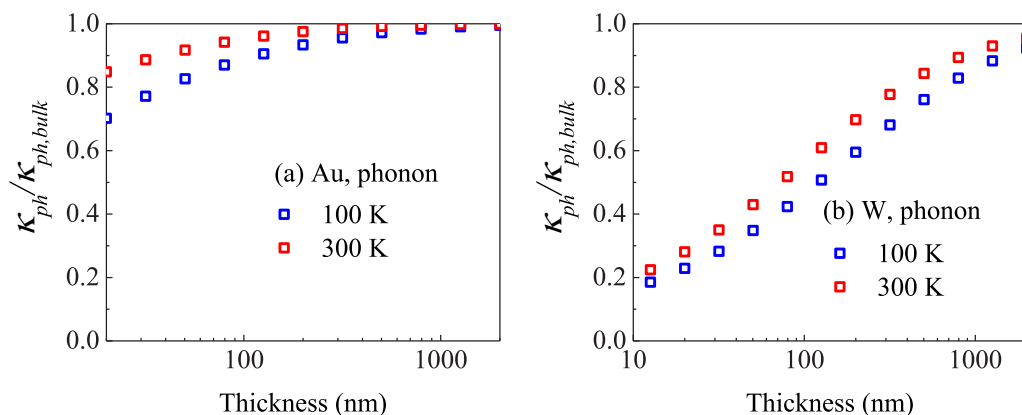

FIG. 5. Thickness H dependent phonon thermal conductivity over bulk phonon thermal conductivity for the (a) Au nanofilm and (b) W nanofilm.
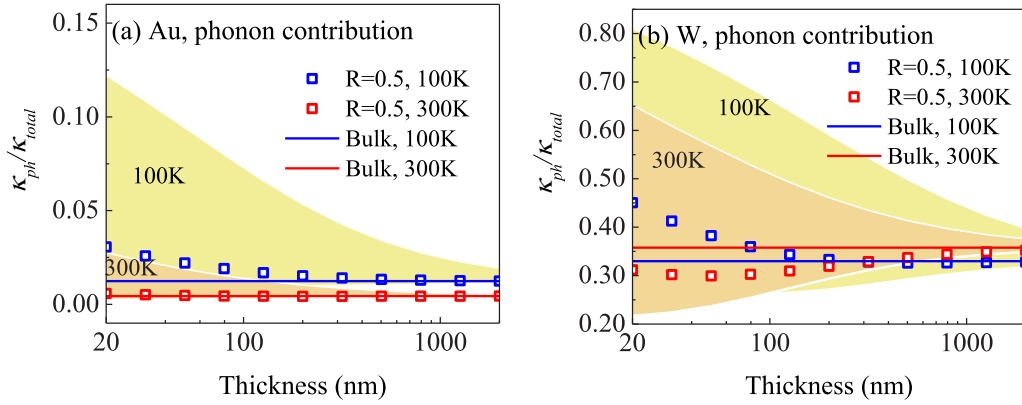
FIG. 6. Thickness H dependent percentage of phonon thermal conductivity contributing to the total thermal conductivity for the (a) Au nanofilm and (b) W nanofilm.

electrons [78], while the latter causes a smaller size effect in phonons than in electrons. This trade-off also varies at different temperatures. When the grain size decreases and the reflection coefficient of electrons increases (high granular nanostructures), the percentage increases and can reach above 80% at 100 K, which is much larger than 33% in bulk W. When the grain size increases and the reflection coefficient of electrons decreases (low granular nanostructures), the percentage decreases and can be less than 30% at 300 K, which is smaller than 35% in bulk W.

IV. VALIDITY OF THE WIEDEMANN-FRANZ LAW

In this section, we study the validity of the Wiedemann-Franz law. We first discuss the Lorentz ratio estimated by the electronic thermal conductivity: $L_e = \kappa_e/\sigma T$. Then, we discuss the Lorentz ratio estimated by the total thermal conductivity: $L = \kappa_{\text{total}}/\sigma T$. All the conclusions about nanofilms can also be applied to nanowires (results are presented in the Supplemental Material [60]).

The Lorentz ratios L_e calculated by the electronic thermal conductivity of bulk Au and bulk W are smaller than the Sommerfeld value (Fig. 7). When the temperature drops, the discrepancy gets larger. Note that this phenomenon is usually

attributed to the inelastic electron-phonon scattering [5,9,28]. However, Ref. [38] showed that the difference between electron momentum relaxation time and energy relaxation time is small in metal Cu and Al when the temperature is higher than 100 K. The inelastic electron-phonon scattering effects can also be ignored in the temperature range of 100–400 K in Au and W, shown in Fig. 10. We attribute the departure in the Lorentz ratio to the energy-dependent electron relaxation time around the Fermi energy. The detailed explanation is shown in the Appendix. The electron relaxation time of bulk Au has weaker energy dependence compared to bulk W (shown in Fig. 11), resulting in a smaller departure in the Lorentz number of Au. Since the range of electron mean free path is narrow, the electron scatterings caused by grain boundary scattering and surface scattering are nearly energy independent. With the addition of such energy-independent scatterings, the energy-dependent behavior of scattering in nanostructures becomes weaker (shown in Fig. 11). Thus, the Lorentz ratio L_e of nanostructures is closer to the Sommerfeld value when the size effect increases, i.e., the thickness and grain size decrease. The Lorentz ratio of an Au nanofilm matches well with the Sommerfeld value in the whole temperature range we studied (100–400 K). In contrast, the Lorentz ratio of a W nanofilm is still smaller than the Sommerfeld
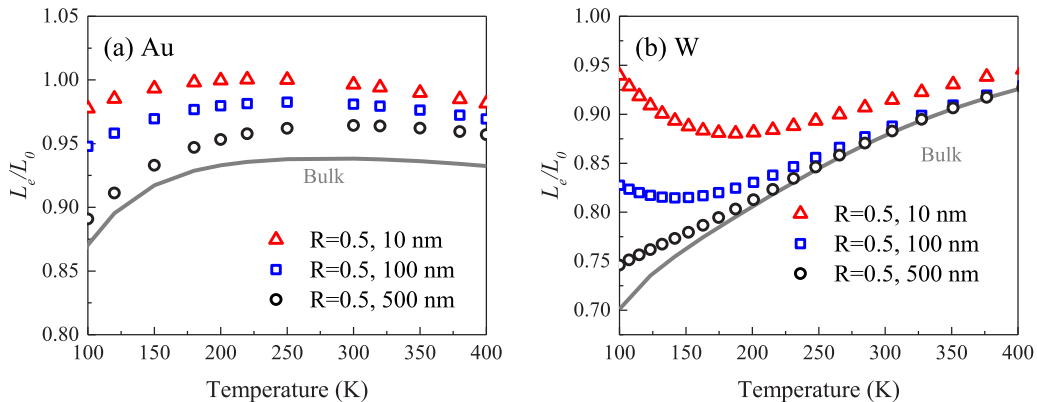

FIG. 7. Temperature dependent Lorentz ratio L_e for the (a) Au nanofilm and (b) W nanofilm. The Lorentz ratio is normalized by Sommerfeld value, as $L_0 = 2.44 \times 10^{-8}$ W Ω/K^2.
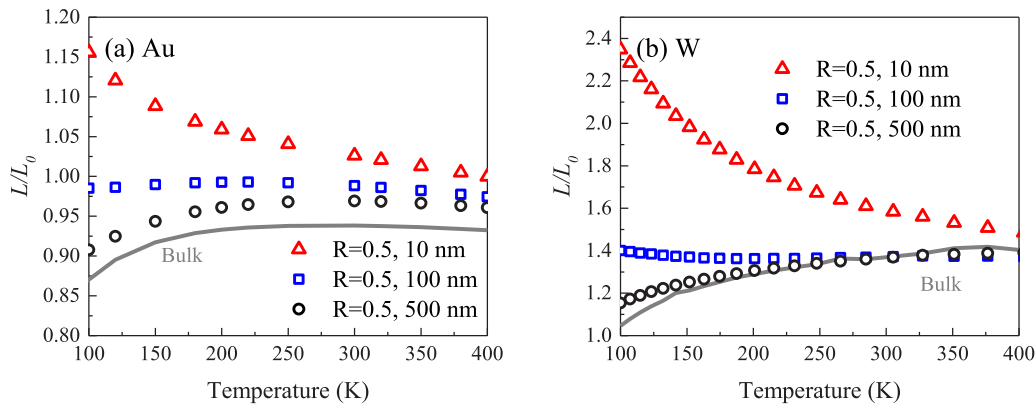
FIG. 8. Temperature dependent Lorentz ratio L for the (a) Au nanofilm, (b) W nanofilm. The Lorentz ratio is normalized by the Sommerfeld value, as $L_0 = 2.44 \times 10^{-8}$ W Ω/K^2.

value due to its energy-dependent electron relaxation time, shown in Fig. 11(b). Overall, the discrepancy is within 30% in W nanofilms.

Since the electronic thermal conductivity is difficult to obtain in experiments, the Lorentz ratio is sometimes estimated by the total thermal conductivity $L = \kappa_{\mathrm{total}}/\sigma T$. The Lorentz ratio L can be larger than the Sommerfeld value due to the additional phonon contribution (Fig. 8). Since the phonon contribution in nanofilms is different from that in bulk metals, the increment of Lorentz ratio L is also different from that in bulk metals. In Au, due to the increment of phonon contribution and the weaker energy-dependent electron scattering, the Lorentz ratio L is larger in nanofilms than in bulk Au. For W, since the phonon contribution in nanofilms has a large range (Fig. 6), the Lorentz ratio L in nanofilms also spans a large range, and the upper limit can reach 2.4 times the Sommerfeld value.

The Au polycrystalline nanofilm has also been studied in experimental studies [5,7,9,27]. The reported Lorentz ratios L are shown in Fig. 9. The reported Lorentz ratios L spans a large range from 3 times to 0.1 times the Sommerfeld value. In these works, L larger than the Sommerfeld value is ascribed to the phonon contribution [7,27], and L smaller than the Som-

merfeld value is explained by the inelastic electron-phonon scattering [5,9]. The Bloch-Grüneisen (BG) model [58,79,80] is also applied to fit the deviation of Lorenz ratio L_e in nanostructures previously [5,10,18]. However, the BG model is not a quantitative model due to the strong assumptions in it, such as the Debye phonon spectrum and electrons are only scattered by longitudinal acoustic phonons [38]. In our model, we rigorously consider the phonon contribution and include the intrinsic inelastic electron-phonon scattering. We also present the range of our predicted results in Fig. 9. The upper limit of the range is the Sommerfeld value plus the phonon contribution (set as 13%, since the percentages we obtained are below 13%). The lower limit is the bulk Lorentz ratio. Some experimental results [5,7,9,27] exceed the range of predicted results. Since we assume that the existence of grain boundaries does not induce inelastic electron-phonon scattering, one possible reason for the deviation is that the high granular nature of the experimental sample induces inelastic electron-phonon scattering [9]. The inelastic scattering can induce the Lorentz ratio value to be the Sommerfeld value multiplied by an efficiency factor, which is within the theoretical limit between 0 and 2 [38,56,58]. This also indicates that the mechanism of electron and phonon scattering at grain boundaries should be further studied. Finally, we note that only a single set of experimental data (Ref. [27]) observed that the Lorentz ratio value exceeds the range of zero to two times and reaches three times the Sommerfeld value, which cannot be explained by inelastic scattering, and the mechanism should be further analyzed.

A recent careful experimental measurement reveals that when excluding the contact resistance, the Lorentz ratio of silver nanowires is close to the Sommerfeld value [11], which is consistent with our findings (silver also has a small phonon contribution, which is similar to Au). It indicates that there may be some uncertainties in earlier experimental measurements due to the challenge in dealing with contact resistance. Thus, to fully understand these effects, further experiments need to be carefully performed.
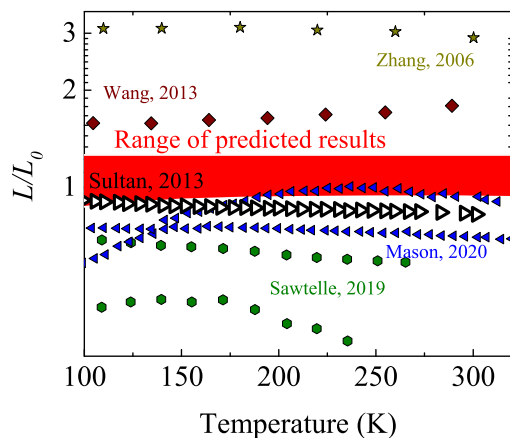

FIG. 9. The range of our predicted and the reported Lorentz ratios for Au nanofilms (normalized by the Sommerfeld value) in previous experimental studies [5,7,9,27,81].

V. CONCLUSIONS

In this study, we use the framework of first-principles calculations combining the Boltzmann transport equation to study the thermal transport in metallic nanostructures. Within

this framework, the mode-by-mode electron and phonon properties are rigorously considered. The size effect and the validity of the Wiedemann-Franz law in Au and W nanostructures are studied.

For the size effect, we show that the thermal conductivity is smaller than the bulk value when the size is in the range of 10–1000 nm. Both the phonon and electronic thermal conductivity decrease with the size. Specifically, the size effect of the electronic thermal conductivity can be well described by the free electron model with an error less than 10%. However, the phonon contribution to the total thermal conductivity is complicated in metallic nanostructures, as it relates to the metals, temperatures, grain properties, and sizes. For Au, the phonon contribution in a thin film is larger than that in bulk metal and can reach up to 15%, which is much larger than 1% in bulk Au. For W, the phonon contribution is in a large range (20–80%), which can be either larger or smaller than the bulk value (∼30%). Roughly, the phonon contribution increases in nanostructures for those metals with small bulk phonon thermal conductivity (like Au), while it can be suppressed in nanostructures for those metals with large bulk phonon thermal conductivity (like W).

By assuming that the grain boundary does not induce inelastic electron-phonon scattering, the Lorentz ratio of nanostructures estimated by the electronic thermal conductivity is between the bulk value and the Sommerfeld value. The Lorentz ratio is closer to the Sommerfeld value when size decreases. In Au and W nanostructures, the Wiedemann-Franz law works well. The Lorentz ratio estimated by total thermal conductivity can be larger than the Sommerfeld value and can reach a large value due to the large phonon contribution. Some reported Lorentz ratios for Au polycrystalline nanofilms exceed the range of our findings: between the Sommerfeld value and the bulk Lorentz ratio. To fully understand these effects, further experiments need to be carefully performed. Moreover, the effect of the grain boundary on the electron-phonon interaction should be further investigated.

APPENDIX: ENERGY-DEPENDENT ELECTRON RELAXATION TIME

In previous works [5,9,28], the departure of the Lorentz ratio from the Sommerfeld value is usually attributed to the inelastic electron-phonon scattering. The same charge carrier holds intrinsically different channels for electrical and heat conduction. Here we present the average electron energy relaxation time and momentum relaxation time to identify the inelastic electron-phonon scattering. The average electron
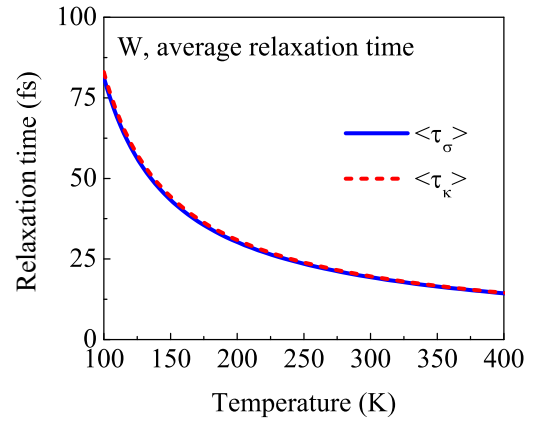

FIG. 10. The average momentum relaxation time (τ_σ) and the energy relaxation time (τ_κ) with different temperatures for W.

relaxation times are calculated from the following expressions [82]:

$$\langle \tau_\sigma \rangle = \frac{\sum_{\mathbf{k}m} \frac{\partial f^0_{\mathbf{k}m}}{\partial \varepsilon_{\mathbf{k}m}} |v_{\mathbf{k}m}|^2 \tau_{\sigma,\mathbf{k}m}}{\sum_{\mathbf{k}m} \frac{\partial f^0_{\mathbf{k}m}}{\partial \varepsilon_{\mathbf{k}m}} |v_{\mathbf{k}m}|^2}, \tag{A1}$$

$$\langle \tau_\kappa \rangle = \frac{\sum_{\mathbf{k}m} \frac{\partial f^0_{\mathbf{k}m}}{\partial \varepsilon_{\mathbf{k}m}} |v_{\mathbf{k}m}|^2 \tau_{\kappa,\mathbf{k}m}}{\sum_{\mathbf{k}m} \frac{\partial f^0_{\mathbf{k}m}}{\partial \varepsilon_{\mathbf{k}m}} |v_{\mathbf{k}m}|^2}. \tag{A2}$$

$\tau_{\sigma,\mathbf{k}m}$ and $\tau_{\kappa,\mathbf{k}m}$ are the mode-by-mode momentum relaxation time and energy relaxation time. Their detailed expressions can be found in Ref. [38]. The two average electron relaxation times are almost identical to each other in the entire temperature range, as shown in Fig. 10. Therefore, the difference between the Lorentz ratio and the Sommerfeld value is not related to the inelastic electron-phonon scattering.

Here, we attribute the departure of the Lorentz ratio from the Sommerfeld value to the energy-dependent electron relaxation time near the Fermi energy [38]. The energy-dependent electron relaxation time is given by

$$\tau(\varepsilon) = \frac{\sum_{\mathbf{k}m} \tau_{\mathbf{k}m} \delta(\varepsilon - \varepsilon_{\mathbf{k}m})}{\sum_{\mathbf{k}m} \delta(\varepsilon - \varepsilon_{\mathbf{k}m})}. \tag{A3}$$

The δ function is approximated by the Gaussian broadening scheme $\delta(x) = \lim_{\eta \to 0} \frac{1}{\sqrt{\pi}} \frac{1}{\eta} e^{-(x/\eta)^2}$. The broadening parameter η is chosen as 0.01 eV. The calculated energy-dependent electron relaxation times are shown in Fig. 11. For the bulk cases, we only consider the electron-phonon scattering and peaks exist in the electron relaxation times of both Au and W at 100 K. The peaks become weaker at higher temperatures. This is an intrinsic behavior of electron and it is attributed to equilibrium distribution functions of electron and phonon [83]. The larger peak in the electron relaxation time results in the more significant failure of the Wiedemann-Franz law. Bulk W holds a larger peak compared to bulk Au at 100 K and the former has significantly smaller Lorentz ratio, shown in Fig. 7. The peaks will decay or disappear in the electron relaxation times of thin films since the electron scattering induced by grain boundary scattering and surface scattering is nearly energy independent. The constant relaxation time
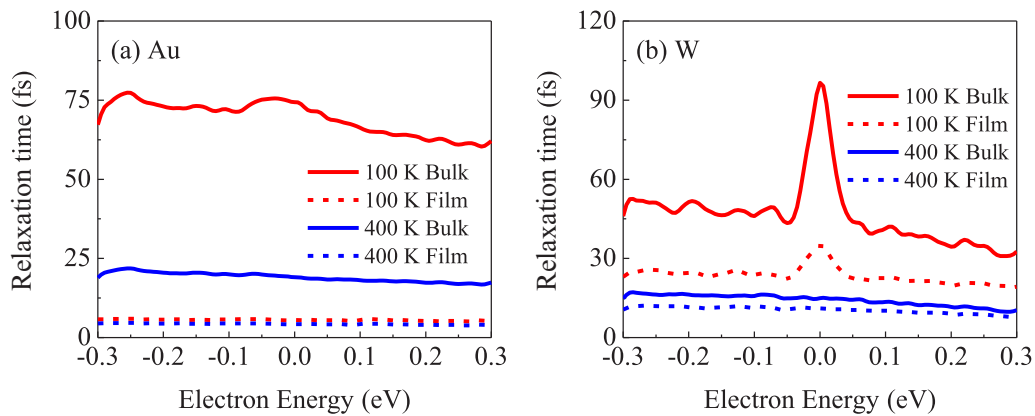
FIG. 11. The energy-dependent electron relaxation time of (a) gold and (b) tungsten at 100 and 400 K with/without grain boundary scattering and surface scattering. The electron energy is normalized to the Fermi energy. The grain size and thickness of the nanofilm are 50 nm. The reflection coefficient is 0.5. The surface scattering is diffuse scattering.

approximation can be applied to cases with energy-independent electron relaxation times. Therefore, the Wiedemann-Franz law is valid in these cases [38]. The peak still exists in the electron relaxation time of the W thin film at 100 K, shown in Fig. 11(b). That is why the departure of Lorentz ratio is observed in the W thin films in Fig. 7(b).

[1] E. C. Walter, K. Ng, M. P. Zach, R. M. Penner, and F. Favier, Microelectron. Eng. **61–62**, 555 (2002).

[2] Y. Xiong and X. Lu, *Metallic Nanostructures* (Springer, Cham, Switzerland, 2015).

[3] A. Facchetti and T. J. Marks, *Transparent Electronics: From Synthesis to Applications* (John Wiley & Sons, Chichester, UK, 2010).

[4] A. L. Moore and L. Shi, Mater. Today **17**, 163 (2014).

[5] S. J. Mason, D. J. Wesenberg, A. Hojem, M. Manno, C. Leighton, and B. L. Zink, Phys. Rev. Mater. **4**, 065003 (2020).

[6] L. Qiu, N. Zhu, Y. Feng, E. E. Michaelides, G. Żyła, D. Jing, X. Zhang, P. M. Norris, C. N. Markides, and O. Mahian, Phys. Rep. **843**, 1 (2020).

[7] H. Wang, J. Liu, X. Zhang, and K. Takahashi, Int. J. Heat Mass Transfer **66**, 585 (2013).

[8] W. Ma and X. Zhang, Int. J. Heat Mass Transfer **58**, 639 (2013).

[9] S. D. Sawtelle and M. A. Reed, Phys. Rev. B **99**, 054304 (2019).

[10] D. Kojda, R. Mitdank, M. Handwerg, A. Mogilatenko, M. Albrecht, Z. Wang, J. Ruhhammer, M. Kroener, P. Woias, and S. F. Fischer, Phys. Rev. B **91**, 024302 (2015).

[11] Y. Zhao, M. L. Fitzgerald, Y. Tao, Z. Pan, G. Sauti, D. Xu, Y. Xu, and D. Li, Nano Lett. **20**, 7389 (2020).

[12] T. Q. Qiu and C. L. Tien, J. Heat Transfer **115**, 842 (1993).

[13] B. Feng, Z. Li, and X. Zhang, Thin Solid Films **517**, 2803 (2009).

[14] B. Feng, Z. Li, and X. Zhang, J. Phys. D: Appl. Phys. **42**, 055311 (2009).

[15] H. Lin, S. Xu, C. Li, H. Dong, and X. Wang Nanoscale **5**, 4652 (2013).

[16] Z. Cheng, L. Liu, S. Xu, M. Lu, and X. Wang, Sci. Rep. **5**, 10718 (2015).

[17] M. Yarifard, J. Davoodi, and H. Rafii-Tabar, Comput. Mater. Sci. **111**, 247 (2016).

[18] A. D. Avery, S. J. Mason, D. Bassett, D. Wesenberg, and B. L. Zink, Phys. Rev. B **92**, 214410 (2015).

[19] G. Chen, *Nanoscale Energy Transport and Conversion: A Parallel Treatment of Electrons, Molecules, Phonons, and Photons* (Oxford University Press, New York, 2005).

[20] D. G. Cahill, P. V. Braun, G. Chen, D. R. Clarke, S. Fan, K. E. Goodson, P. Keblinski, W. P. King, G. D. Mahan, A. Majumdar, H. J. Maris, S. R. Phillpot, E. Pop, and L. Shi, Appl. Phys. Rev. **1**, 011305 (2014).

[21] J. J. Plombon, E. Andideh, V. M. Dubin, and J. Maiz, Appl. Phys. Lett. **89**, 113124 (2006).

[22] T. Sun, B. Yao, A. P. Warren, K. Barmak, M. F. Toney, R. E. Peale, and K. R. Coffey, Phys. Rev. B **79**, 041402 (2009).

[23] C. Shao, Q. Rong, N. Li, and H. Bao, Phys. Rev. B **98**, 155418 (2018).

[24] K. Fuchs, Math. Proc. Cambridge Philos. Soc. **34**, 100 (1938).

[25] A. F. Mayadas and M. Shatzkes, Phys. Rev. B **1**, 1382 (1970).

[26] X. Zhang, H. Xie, M. Fujii, H. Ago, K. Takahashi, T. Ikuta, H. Abe, and T. Shimizu, Appl. Phys. Lett. **86**, 171912 (2005).

[27] Q. G. Zhang, B. Y. Cao, X. Zhang, M. Fujii, and K. Takahashi, Phys. Rev. B **74**, 134109 (2006).

[28] N. Stojanovic, D. H. S. Maithripala, J. M. Berg, and M. Holtz, Phys. Rev. B **82**, 075418 (2010).

[29] N. Yang, T. Luo, K. Esfarjani, A. Henry, Z. Tian, J. Shiomi, Y. Chalopin, B. Li, and G. Chen, J. Comput. Theor. Nanosci. **12**, 168 (2015).

[30] G. V. Chester and A. Thellung, Proc. Phys. Soc. **77**, 1005 (1961).

[31] F. Völklein, H. Reith, T. W. Cornelius, M. Rauber, and R. Neumann, Nanotechnology **20**, 325706 (2009).

[32] J. Wang, Z. Wu, C. Mao, Y. Zhao, J. Yang, and Y. Chen, Sci. Rep. **8**, 4862 (2018).

[33] J. Wang, H. Yu, T. Walbert, M. Antoni, C. Wang, W. Xi, F. Muench, J. Yang, and Y. Chen, Nanotechnology **30**, 455706 (2019).

[34] D. Choi, C. S. Kim, D. Naveh, S. Chung, A. P. Warren, N. T. Nuhfer, M. F. Toney, K. R. Coffey, and K. Barmak, Phys. Rev. B **86**, 045432 (2012).

[35] D. Gall, J. Appl. Phys. **127**, 050901 (2020).

[36] Y. Chen, J. Ma, and W. Li, Phys. Rev. B **99**, 020305 (2019).

[37] Z. Tong, S. Li, X. Ruan, and H. Bao, Phys. Rev. B **100**, 144306 (2019).

[38] S. Li, Z. Tong, X. Zhang, and H. Bao, Phys. Rev. B **102**, 174306 (2020).

[39] S. Li, A. Wang, Y. Hu, X. Gu, Z. Tong, and H. Bao, Mater. Today Phys. **15**, 100256 (2020).

[40] B. Fu, K. D. Parrish, H. Y. Kim, G. Tang, and A. J. H. McGaughey, Phys. Rev. B **101**, 045417 (2020).

[41] S. Bose, C. Galande, S. P. Chockalingam, R. Banerjee, P. Raychaudhuri, and P. Ayyub, J. Phys.: Condens. Matter **21**, 205702 (2009).

[42] R. C. Munoz and C. Arenas, Appl. Phys. Rev. **4**, 011102 (2017).

[43] J. Y. Murthy and S. R. Mathur, J. Heat Transfer **124**, 1176 (2002).

[44] Y. Hu, T. Feng, X. Gu, Z. Fan, X. Wang, M. Lundstrom, S. S. Shrestha, and H. Bao, Phys. Rev. B **101**, 155308 (2020).

[45] D. Josell, S. H. Brongersma, and Z. Tőkei, Annu. Rev. Mater. Res. **39**, 231 (2009).

[46] S. B. Soffer, J. Appl. Phys. **38**, 1710 (1967).

[47] J. R. Sambles, Thin Solid Films **106**, 321 (1983).

[48] R. L. Graham, G. B. Alers, T. Mountsier, N. Shamma, S. Dhuey, S. Cabrini, R. H. Geiss, D. T. Read, and S. Peddeti, Appl. Phys. Lett. **96**, 042116 (2010).

[49] T. Sun, B. Yao, A. P. Warren, K. Barmak, M. F. Toney, R. E. Peale, and K. R. Coffey, Phys. Rev. B **81**, 155454 (2010).

[50] H. K. Liu, Y. Lin, and S. N. Luo, J. Phys. Chem. C **118**, 24797 (2014).

[51] C. Kimmer, S. Aubry, A. Skye, and P. K. Schelling, Phys. Rev. B **75**, 144105 (2007).

[52] A. Bietsch and B. Michel, Appl. Phys. Lett. **80**, 3346 (2002).

[53] J. S. Chawla, F. Gstrein, K. P. O'Brien, J. S. Clarke, and D. Gall, Phys. Rev. B **84**, 235423 (2011).

[54] A. Bagri, S. P. Kim, R. S. Ruoff, and V. B. Shenoy, Nano Lett. **11**, 3917 (2011).

[55] Y. Lu and J. Guo, Appl. Phys. Lett. **101**, 043112 (2012).

[56] A. Lavasani, D. Bulmash, and S. Das Sarma, Phys. Rev. B **99**, 085104 (2019).

[57] R. B. Ganvir, P. V. Walke, and V. M. Kriplani, Renew. Sustain. Energy Rev. **75**, 451 (2017).

[58] T. M. Tritt, *Thermal Conductivity: Theory, Properties, and Applications* (Springer Science & Business Media, New York, 2005).

[59] D. A. Broido, M. Malorny, G. Birner, N. Mingo, and D. A. Stewart, Appl. Phys. Lett. **91**, 231922 (2007).

[60] See Supplemental Material at http://link.aps.org/supplemental/10.1103/PhysRevB.103.104301 for details on (i) the deviation of the expression of thermal conductivity, (ii) wavelength accu-

mulation function, (iii) average mean free path of Au and W, and (iv) results for nanowires.

[61] J. M. Ziman, *Electrons and Phonons: The Theory of Transport Phenomena in Solids* (Oxford University Press, New York, 2001).

[62] Y. Wang, Z. Lu, and X. Ruan, J. Appl. Phys. **119**, 225109 (2016).

[63] A. K. Vallabhaneni, D. Singh, H. Bao, J. Murthy, and X. Ruan, Phys. Rev. B **93**, 125432 (2016).

[64] G. D. Mahan, *Many-Particle Physics* (Springer Science & Business Media, New York, 2000).

[65] S. Wen, J. Ma, A. Kundu, and W. Li, Phys. Rev. B **102**, 064303 (2020).

[66] W. Li, Phys. Rev. B **92**, 075405 (2015).

[67] P. Giannozzi, S. Baroni, N. Bonini, M. Calandra, R. Car, C. Cavazzoni, D. Ceresoli, G. L. Chiarotti, M. Cococcioni, I. Dabo, A. Dal Corso, S. De Gironcoli, S. Fabris, G. Fratesi, R. Gebauer, U. Gerstmann, C. Gougoussis, A. Kokalj, M. Lazzeri, L. Martin-Samos *et al.*, J. Phys.: Condens. Matter **21**, 395502 (2009).

[68] J. P. Perdew and Y. Wang, Phys. Rev. B **98**, 195128 (2018).

[69] J. P. Perdew, K. Burke, and M. Ernzerhof, Phys. Rev. Lett. **78**, 1396 (1997).

[70] W. Li, J. Carrete, N. A. Katcho, and N. Mingo, Comput. Phys. Commun. **185**, 1747 (2014).

[71] J. Noffsinger, F. Giustino, B. D. Malone, C. H. Park, S. G. Louie, and M. L. Cohen, Comput. Phys. Commun. **181**, 2140 (2010).

[72] Y. S. Touloukian, R. W. Powell, C. V. Ha, and P. G. Klemens, *Thermophysical Properties of Matte*, The TPRC Data Series. Vol. 1, Thermal Conductivity - Metallic Elements and Alloys (IFI/Plenum, New York, 1970) Vol. 1.

[73] F. Yang and C. Dames, Phys. Rev. B **87**, 035437 (2013).

[74] S. Zahiri, Z. Xu, Y. Hu, H. Bao, and Y. Shen, Int. J. Heat Mass Transfer **138**, 267 (2019).

[75] P. Zheng and D. Gall, J. Appl. Phys. **122**, 135301 (2017).

[76] E. Fawcett and D. Griffiths, J. Phys. Chem. Solids **23**, 1631 (1962).

[77] C. Kittel and D. F. Holcomb, *Introduction to Solid State Physics* (Wiley, New York, 1967).

[78] Y. Chen, J. Ma, S. Wen, and W. Li, Npj Comput. Mater. **5**, 98 (2019).

[79] F. Bloch, Z. Phys. **52**, 555 (1929).

[80] E. Grüneisen, Ann. Phys. **408**, 530 (1933).

[81] R. Sultan, A. D. Avery, J. M. Underwood, S. J. Mason, D. Bassett, and B. L. Zink, Phys. Rev. B **87**, 214305 (2013).

[82] J. Coulter, R. Sundararaman, and P. Narang, Phys. Rev. B **98**, 115130 (2018).

[83] F. Rittweger, N. F. Hinsche, and I. Mertig, J. Phys.: Condens. Matter **29**, 355501 (2017).